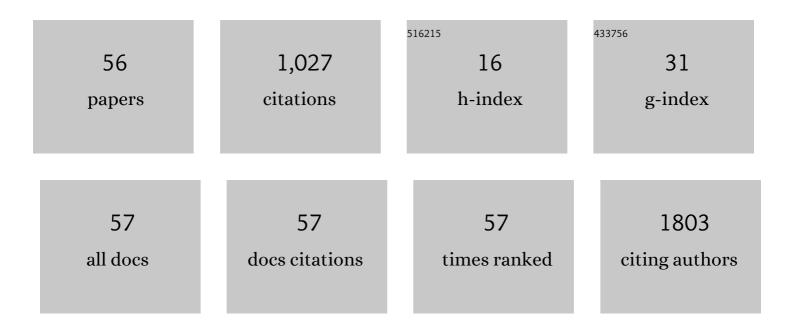
## Ann Chiaramonti

List of Publications by Year in descending order

Source: https://exaly.com/author-pdf/2362483/publications.pdf Version: 2024-02-01



#	Article	IF	CITATIONS
1	Optical Scattering Characteristics of 3-D Lunar Regolith Particles Measured Using X-Ray Nano Computed Tomography. IEEE Geoscience and Remote Sensing Letters, 2022, 19, 1-5.	1.4	2
2	Towards data-driven next-generation transmission electron microscopy. Nature Materials, 2021, 20, 274-279.	13.3	130
3	Extreme Ultraviolet Radiation Pulsed Atom Probe Tomography of III-Nitride Semiconductor Materials. Journal of Physical Chemistry C, 2021, 125, 2626-2635.	1.5	3
4	Comparative Apex Electrostatics of Atom Probe Tomography Specimens. Journal of Electronic Materials, 2021, 50, 3022-3029.	1.0	4
5	On the Voltage and Bowl Correction of Trigger-Uncorrelated Multihit Events. Microscopy and Microanalysis, 2021, 27, 412-415.	0.2	0
6	Atom probe tomography. Nature Reviews Methods Primers, 2021, 1, .	11.8	131
7	Correcting Systematic Energy Deficits in the Laser-pulsed Atom Probe Mass Spectrum of SiO2. Microscopy and Microanalysis, 2020, 26, 2880-2881.	0.2	0
8	An algorithm for correcting systematic energy deficits in the atom probe mass spectra of insulating samples. Ultramicroscopy, 2020, 213, 112995.	0.8	7
9	Field Ion Emission in an Atom Probe Microscope Triggered by Femtosecond-Pulsed Coherent Extreme Ultraviolet Light. Microscopy and Microanalysis, 2020, 26, 258-266.	0.2	11
10	Atom Probe Tomography Using a Wavelength-Tunable Femtosecond-Pulsed Coherent Extreme Ultraviolet Light Source. Microscopy and Microanalysis, 2019, 25, 314-315.	0.2	0
11	A Three-Dimensional Atom Probe Microscope Incorporating a Wavelength-Tuneable Femtosecond-Pulsed Coherent Extreme Ultraviolet Light Source. MRS Advances, 2019, 4, 2367-2375.	0.5	11
12	An Experimental Scattering Matrix for Lunar Regolith Simulant JSC-1A at Visible Wavelengths. Astrophysical Journal, Supplement Series, 2018, 235, 19.	3.0	22
13	Quantifying the 3-Dimensional Shape of Lunar Regolith Particles Using X-Ray Computed Tomography and Scanning Electron Microscopy at Sub-Î <sup>3</sup> Resolution. Microscopy and Microanalysis, 2017, 23, 2194-2195.	0.2	7
14	Chemical Segregation and Microstructural Evolution of Fiber Laser Welded Low Carbon Sheet Steel. , 2017, , .		0
15	Introducing a New NIST Reference Material: Multiwall Carbon Nanotube Soot. Microscopy and Microanalysis, 2016, 22, 450-451.	0.2	1
16	Behavior of molecules and molecular ions near a field emitter. New Journal of Physics, 2016, 18, 033031.	1.2	130
17	Timescale of silver nanoparticle transformation in neural cell cultures impacts measured cell response. Journal of Nanoparticle Research, 2015, 17, 1.	0.8	1
18	Localization and Number of Au Nanoparticles in Optically Indexed Cells by FIB Tomography. Microscopy and Microanalysis, 2015, 21, 411-412.	0.2	0

#	Article	IF	CITATIONS
19	Morphological and Electrical Characterization of MWCNT Papers and Pellets. Journal of Research of the National Institute of Standards and Technology, 2015, 120, 304.	0.4	8
20	Transition from Order to Configurational Disorder for Surface Reconstructions on <mml:math xmlns:mml="http://www.w3.org/1998/Math/MathML" display="inline"&gt;<mml:mrow><mml:msub><mml:mrow><mml:mi>SrTiO</mml:mi></mml:mrow><mml:mrow> Physical Review Letters, 2015, 114, 226101.</mml:mrow></mml:msub></mml:mrow></mml:math 	<mm<b>1:mn&gt;:</mm<b>	3<
21	Stability and phase transfer of catalytically active platinum nanoparticle suspensions. Journal of Nanoparticle Research, 2015, 17, 1.	0.8	4
22	Gold Nanoparticle Quantitation by Whole Cell Tomography. ACS Nano, 2015, 9, 11792-11799.	7.3	8
23	Atomically thin layers of B–N–C–O with tunable composition. Science Advances, 2015, 1, e1500094.	4.7	55
24	Suppression of spin pumping between Ni80Fe20 and Cu by a graphene interlayer. Journal of Applied Physics, 2015, 117, 213907.	1.1	7
25	Citrate-stabilized gold nanoparticles as negative controls for measurements of neurite outgrowth. Toxicology in Vitro, 2015, 29, 187-194.	1.1	5
26	Dominant thermal boundary resistance in multi-walled carbon nanotube bundles fabricated at low temperature. Journal of Applied Physics, 2014, 116, 023514.	1.1	6
27	Engineering plant cell walls: tuning lignin monomer composition for deconstructable biofuel feedstocks or resilient biomaterials. Green Chemistry, 2014, 16, 2627.	4.6	60
28	Applicability of post-ionization theory to laser-assisted field evaporation of magnetite. Applied Physics Letters, 2014, 105, .	1.5	24
29	Understanding the High-Temperature Mechanical Properties of A710 (HSLA-80) Steel With Use of Complementary Atom Probe Tomography and Electron Microscopy. Microscopy and Microanalysis, 2014, 20, 954-955.	0.2	1
30	Correlating Multiscale Measurements of Nanoparticles in Primary Cells. Microscopy and Microanalysis, 2014, 20, 976-977.	0.2	2
31	Electron and Helium Ion Imaging of Arabidopsis Affected by Genetic Mutation and Thermochemical Treatment for Biofuel Applications. Microscopy and Microanalysis, 2014, 20, 1338-1339.	0.2	1
32	Failure Analysis and Reliability of Low-Temperature-Grown Multi-Wall Carbon Nanotube Bundles Integrated as Vias in Monolithic Three-Dimensional Integrated Circuits. Microscopy and Microanalysis, 2014, 20, 1762-1763.	0.2	0
33	Statistical sampling of carbon nanotube populations by thermogravimetric analysis. Analytical and Bioanalytical Chemistry, 2013, 405, 8207-8213.	1.9	8
34	Towards the Integration of Carbon Nanotubes as Vias in Monolithic Three-Dimensional Integrated Circuits. Japanese Journal of Applied Physics, 2013, 52, 04CB02.	0.8	6
35	Epitaxial (111) films of Cu, Ni, and CuxNiy on αâ^'Al2O3 (0001) for graphene growth by chemical vapor deposition. Journal of Applied Physics, 2012, 112, .	1.1	51
36	Contact resistance of low-temperature carbon nanotube vertical interconnects. , 2012, , .		5

36  $Contact\ resistance\ of\ low-temperature\ carbon\ nanotube\ vertical\ interconnects.\ ,\ 2012,\ ,\ .$ 

ANN CHIARAMONTI

#	Article	IF	CITATIONS
37	Effects of elemental distributions on the behavior of MgO-based magnetic tunnel junctions. Journal of Applied Physics, 2011, 109, 103909.	1.1	15
38	Accelerated reliability testing of highly aligned single-walled carbon nanotube networks subjected to DC electrical stressing. Nanotechnology, 2011, 22, 265713.	1.3	11
39	Homoepitaxial n-core: p-shell gallium nitride nanowires: HVPE overgrowth on MBE nanowires. Nanotechnology, 2011, 22, 465703.	1.3	10
40	Effect of annealing and applied bias on barrier shape in CoFe/MgO/CoFe tunnel junctions. Physical Review B, 2011, 83, .	1.1	16
41	Enhanced magnetoresistance in naturally oxidized MgO-based magnetic tunnel junctions with ferromagnetic CoFe/CoFeB bilayers. Applied Physics Letters, 2011, 98, 232506.	1.5	12
42	Reliability Testing of Advanced Interconnect Materials. , 2011, , .		1
43	The Fe3O4 origin of the "Biphase―reconstruction on α-Fe2O3(0001). Surface Science, 2009, 603, 2574-2579.	0.8	45
44	The small unit cell reconstructions of SrTiO3(111). Surface Science, 2009, 603, 2179-2187.	0.8	33
45	In situ TEM studies of local transport and structure in nanoscale multilayer films. Ultramicroscopy, 2008, 108, 1529-1535.	0.8	11
46	Time, temperature, and oxygen partial pressure-dependent surface reconstructions on SrTiO3(111): A systematic study of oxygen-rich conditions. Surface Science, 2008, 602, 3018-3025.	0.8	23
47	Transmission Electron Microscopy of Multilayer Thin Films. Annual Review of Materials Research, 2008, 38, 559-584.	4.3	28
48	Effects of annealing on local composition and electrical transport correlations in MgO-based magnetic tunnel junctions. Applied Physics Letters, 2008, 93, .	1.5	30
49	Magnetic Linear Dichroism Probed by High Momentum Resolution EELS. Microscopy and Microanalysis, 2008, 14, 1366-1367.	0.2	1
50	In-situ Structure and Transport Correlations in Magnetic Tunnel Junctions. Microscopy and Microanalysis, 2007, 13, .	0.2	2
51	Comparison of the Chemical Heterogeneities and Microstructure Between CoFeB/MgO/CoFeB and CoFeB/Al-O/CoFeB Magnetic Tunnel Junctions. Microscopy and Microanalysis, 2007, 13, .	0.2	0
52	Charge Compensated Perovskite Polar Surface: SrTiO3(111)-3x3. Microscopy and Microanalysis, 2006, 12, 1230-1231.	0.2	2
53	Controlled Nanoscale Morphology of Hematite (0001) Surfaces Grown by Chemical Vapor Transport. Advanced Materials, 2005, 17, 1765-1768.	11.1	17
54	Impurity stabilized near-surface phase on ion bombarded α-Fe2O3(0001). Surface Science, 2005, 586, 38-44.	0.8	7

#	Article	IF	CITATIONS
55	Atomic Resolution Transmission Electron Microscopy of Surfaces. Journal of Materials Research, 2005, 20, 1619-1627.	1.2	12
56	Optical Floating Zone Growth of Single Crystal α-Fe2O3from a CaFe4O7-Based Solvent. Crystal Growth and Design, 2004, 4, 749-753.	1.4	6